ICSV14
Cairns • Australia
9-12 July, 2007

14th International Congress on Sound & Vibration

DYNAMICS OF PIEZOCERAMICS-BASED MASS AND FORCE ACTUATORS FOR ROTATING MACHINES

Peter Sloetjes, Andre de Boer and Peter van der Hoogt

University of Twente, Faculty of Engineering Technology, Applied Mechanics Section
Drienerlolaan 5, 7500AE, Enschede, The Netherlands
p.j.sloetjes@ctw.utwente.nl

Abstract

In the past decade, it has become more and more common to install active vibration control devices on rotating systems like grinding machines, tooling centers, industrial fans and drive shafts. In the present research, two innovative actuation concepts for such devices are evaluated. The first device is a force actuator based on piezoceramic fibers, which has a low power consumption and high dynamic range. The second device is a mass redistribution actuator based on two piezoelectric ultrasonic motors, which is smaller and faster than conventional electromagnetic devices. At the basis of the analysis are rotor dynamic finite element models including actuators, sensors and feedback controllers. In simulations and experiments with device one, feedback control and scheduled feedforward control are considered. It is shown experimentally that the unbalance response at a critical speed can be reduced by some 97%. In experiments with device two, the positioning speed is determined.

1. INTRODUCTION

The performance of high speed rotating machinery (e.g. grinding machines, tooling centers, textile machines, industrial fans and drive shafts) can often be improved by active vibration control (AVC). Typically, mass redistribution actuators are used to correct time-varying unbalance, while force actuators are used to counteract external disturbances or destabilizing phenomena of high speed rotor systems ([1]). Since AVC devices, like most machine components, must often satisfy strict requirements on size, cost and power consumption, there is an incessant urge to develop smaller, simpler and/or more efficient devices. This paper focuses on two rotor-fixed AVC devices that employ piezoceramic actuators:

- MFC force actuator. Macro fiber composites (MFC's) from Smart Material Corporation are piezoceramic fiber actuators with interdigitated electrodes, which are known for their conformability, performance and low power consumption during static control. A rotor force actuator is created by fixing four MFC actuators (140x3x0.2mm) to four sides of a flexible rotor (Figure 1a). Supplying opposite voltages to the electrodes of

two facing actuators induces surface stresses which are equivalent to bending moments.

- PUM mass actuator. Piezoelectric ultrasonic motors (PUM's) from Shinsei Corporation Inc. are piezoelectric resonance motors with friction transmission, which are known for their compactness, self-locking design and high acceleration and torque. A rotor mass redistribution actuator is created by pressing two revolvable rings with known unbalance to the front of the rotor-fixed driver rings (∅30mm) which at their back have piezoceramic sheets with patterned electrodes (Figure 1b). Supplying two high frequency voltages to a driver ring induces a travelling bending mode with elliptic surface motion which moves the corresponding balancer ring via contact friction.

The MFC and PUM actuators are evaluated in a typical rotor dynamics setup (Figure 1c). The flexible rotor in this setup is 1m long, with end pieces of ∅15mm, a mid piece of ∅25mm and a flywheel of ∅150mm. The transverse stiffness of the bearing supports is adjustable, such that an anisotropic stator stiffness condition can be investigated.

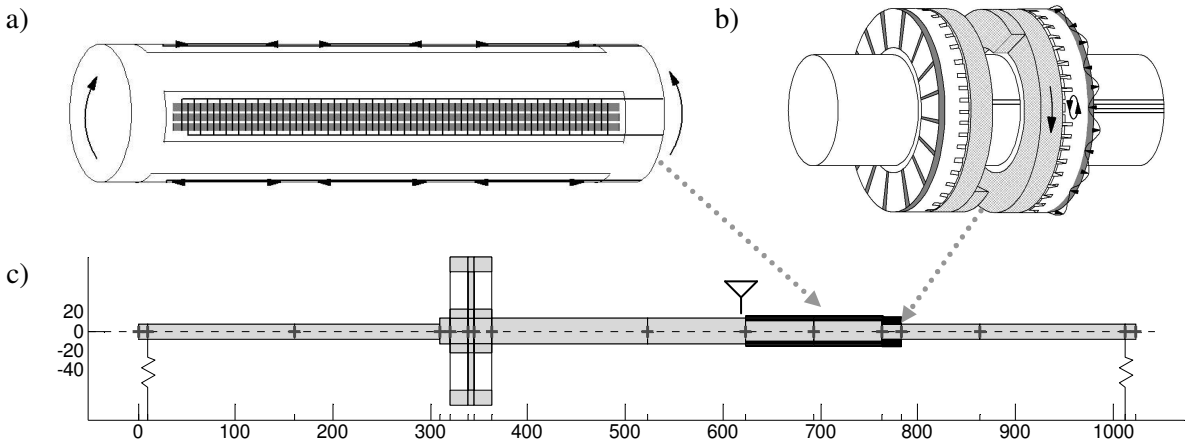

Figure 1. a) MFC force actuator (drawing). b) PUM mass actuator (drawing).
c) Rotor setup (section view of Matlab finite element model).

2. ACTIVE ROTOR MODEL

2.1 Rotor dynamic model

The equation of motion for a discretized model of an axi-symmetric rotor with anisotropic stator in terms of complex coordinates and property matrices is written as (see [2],[3]):

$$\mathbf{M}\ddot{\mathbf{x}}^s+[\mathbf{C}^s+\mathbf{C}^r-i\Omega\mathbf{G}]\dot{\mathbf{x}}^s+[\mathbf{K}^s+\mathbf{K}^r\pm i\mathbf{H}^r-i\Omega\mathbf{C}^r]\mathbf{x}^s+\mathbf{C}^{sd}\bar{\dot{\mathbf{x}}}^s+\mathbf{K}^{sd}\bar{\mathbf{x}}^s=g\,\mathbf{m}+e^{i\Omega t}\Omega^2\mathbf{e}+\mathbf{f}_q^s+\mathbf{f}_p^s \qquad (1)$$

The rotor speed Ω is the time derivative of rotor rotation angle θ. The complex exponential is denoted e^{ix}, with $i^2=-1$ and $\bar{}$ denoting complex conjugation. Vectors $\mathbf{x}^s=\mathbf{x}_x^s+i\mathbf{x}_y^s$, $\mathbf{e}=\mathbf{e}_x^r+i\mathbf{e}_y^r$, $\mathbf{m}$, $\mathbf{f}_q^s=\mathbf{f}_{qx}^s+i\mathbf{f}_{qy}^s$ and $\mathbf{f}_p^s=\mathbf{f}_{px}^s+i\mathbf{f}_{py}^s$ are the degrees of freedom, nodal unbalance, nodal mass, and nodal MFC and PUM actuation forces, respectively, with g the gravitational acceleration. Matrices **M**, **G**, **C**, **K** and **H** are the inertia, gyroscopic, damping, stiffness and hysteresis matrices. Superscripts s and r denote properties of the stator and the rotor. Superscript d denotes properties which are different for the stator principal directions.

A rotor dynamics code in Matlab was developed for numerical analysis. An indication of the dynamics of the setup is given for a model with anisotropic stator stiffness, viscous stator and rotor damping and no rotor hysteresis nor actuation forces. The first two mode shapes at zero speed are shown in Figure 2, while a Campbell diagram is shown in Figure 3a. The frequencies of the first pair of forward/backward modes are nearly equal (21.5Hz / 22.3Hz) and constant, while the frequencies of the second mode pair are significantly different (92.6Hz / 98.2Hz) and speed-dependent due to the gyroscopic effect.

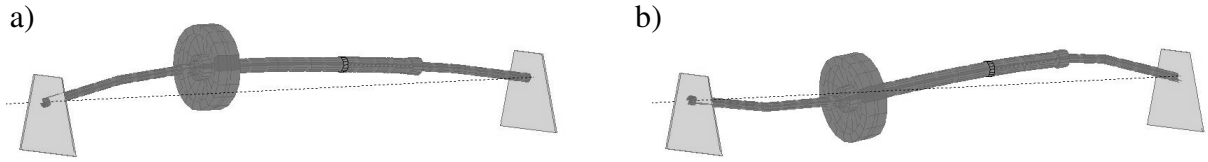

Figure 2. a) First mode shape and b) second mode shape.

2.2 MFC actuator model

The mechanical stiffness of the MFC actuators with short circuit electrodes is included in the rotor stiffness matrix; the stiffness increase due to open circuit electrodes (dielectric stiffening) is considered negligible. The electrodes of each pair of facing MFC actuators are connected in parallel, such that one actuation voltage can be supplied for each bending plane: $v=v_x+iv_y$. In the case of active control, v is imposed by a voltage amplifier (eq. 2a). In case v is free and only parallel resistances R_q are connected to each actuator pair, the actuator charges $q=q_x+iq_y$ obey a balance equation (eq. 2b) (see [6]):

$$\mathbf{f}_q^s = K_q \mathbf{l}_q v\, e^{i\Omega t} \tag{2a}$$

$$R_q \dot{q} + C_q^{-1} q - K_q \mathbf{l}_q^T \mathbf{x}^r = 0 \tag{2b}$$

In these equations, location vector $\mathbf{l}_q$ is set to ±1 at the rotational degrees of freedom where the effective actuator torques apply. C_q, K_q, and R_q are the capacitance at constant strain, piezoelectric torque-voltage coupling constant and parallel resistance, respectively, for each actuator pair. C_q is a function of geometry, dielectric constant e_{33} and electromechanical coupling constant k_{33} and is equal to 3.53nF. K_q is a function of geometry, short circuit elastic modulus Y_3 and piezoelectric constant d_{33} and is equal to 0.92mNm/V. The 3-direction is the MFC fiber direction. The actuation voltages should be in the range of ±500V.

2.3 PUM actuator model

The position of the PUM actuators is marked by +1 in location vector $\mathbf{l}_p$. At this position, actuation force $\mathbf{f}_p^s$ applies which is required for the centripetal acceleration of the balancer weights with mass m_p that are fixed at radial distance d_p to balancer ring n (=1,2) which has rotation angle ϕ_n (eq. 3a). Each balancer ring has rotational inertia J and is driven by a torque M_n which is a nonlinear function of the sinusoidal excitation voltages v_{nc} and v_{ns} and of the contact pressure σ_n (and several other parameters, see [4][5]) (eq. 3b):

$$\mathbf{f}_p^s = d_p m_p \mathbf{l}_p \Omega^2 e^{i(\Omega t+\phi_1+\phi_2)} \tag{3a}$$

$$J\ddot{\phi}_n = M_n\left(\tfrac{1}{2}\left|v_{nc}+v_{ns}\right|, \angle(v_{nc}, v_{ns}), \sigma_n\right) \qquad \text{with} \qquad n=1,2 \tag{3b}$$

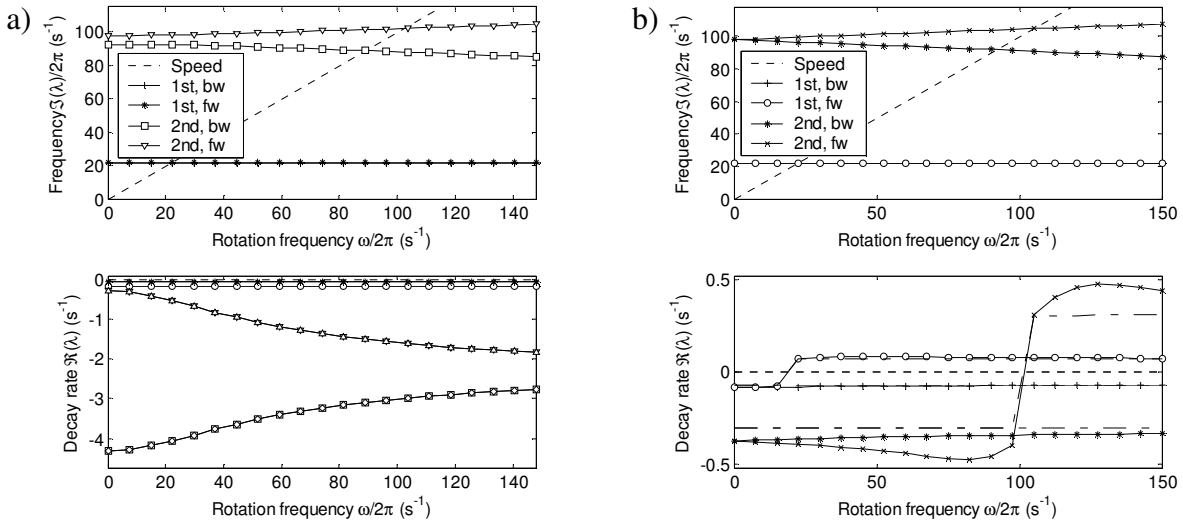

Figure 3. a) Campbell diagram for model with anisotropic stator, viscous stator and rotor damping. b) Campbell diagram for model with isotropic stator, without stator damping, with hysteretic rotor damping, either with (—) or without (-·-) shunt damping.

3. FORCE ACTUATION

3.1 Undesired shunt damping

It is well known that rotor-fixed components may contribute to the rotor damping and hence may have a destabilizing effect on modes with frequencies that are lower than the rotor speed ([2]). In the case of rotor-fixed piezoelectric force actuators, significant damping may be due to resistive dissipation of strain-induced currents, known as 'shunt damping'. The effect of unintentional shunt damping on the rotor stability is quantified for a model with isotropic stator stiffness, no stator damping, but with rotor hysteresis and shunt damping. To this end, complex eigenvalues λ_n are solved from the following state space equation:

$$\dot{\mathbf{z}} = \mathbf{A}(\Omega)\,\mathbf{z} \qquad \mathbf{A}(\Omega) = \begin{bmatrix} -\mathbf{M}^{-1}[-i\,\Omega\mathbf{G}] & -\mathbf{M}^{-1}[\mathbf{K}^m \mp i\,\mathbf{H}^r] & -\mathbf{M}^{-1}\mathbf{l}_q K_q \\ [\mathbf{I}] & [\mathbf{0}] & \{\mathbf{0}\} \\ \{\mathbf{0}\} & K_q R_q^{-1}\mathbf{l}_v^T & i\,\Omega - (R_q C_q)^{-1} \end{bmatrix} \qquad \mathbf{z} = \begin{Bmatrix} \dot{\mathbf{x}}^s \\ \mathbf{x}^s \\ q^s \end{Bmatrix} \tag{4}$$

In this equation, a fictitious state $q^s = e^{i\Omega t} q$ is employed. Matrix $\mathbf{H}^r$ is assembled from the rotor element stiffness matrices multiplied by their respective material loss factors (mostly steel with loss factor 0.001). The sign in front of $i\mathbf{H}^r$ is equal to $sgn(\Im(\lambda_n)-\Omega)$, the direction of circular rotor straining, and is selected correctly for any speed only after solving the eigenvalue problem for both signs (see [2]). Shunt damping is maximized for $\omega = \Im(\lambda_1) = 22\text{Hz}$ by choosing $R_q = (1-k_{33}^2)^{0.5}(\omega C_q)^{-1}$ (see [6]). The eigenvalues of the first two forward / backward mode pairs, with and without shunt damping, are shown in Figure 3b. The jumps in $\Re(\lambda)$ are due to the hysteresis changing its effective direction. Maximum shunt damping is present at $\Omega = \Im(\lambda_1) \pm \omega = 0\text{Hz} / 44\text{Hz}$ (first mode) and $\Omega = \Im(\lambda_2) \pm \omega \approx 76\text{Hz} / 120\text{Hz}$ (second mode). Shunt damping has the same order of magnitude as hysteretic damping. Given the fact that the amount of (stabilizing) stator damping is often small, it is concluded that the circuits that are connected to the actuators should be designed so as to avoid maximum dissipation.

3.2 Derivative feedback control

Active control of rotor-fixed force actuators can be used to counteract disturbances, improve stability and/or cancel unbalance [7][8]. In this section, it is focused on the suppression of rotor vibration due to unbalance at critical speeds. A preparatory investigation made clear that a combination of speed-scheduled active balancing and damping is very effective.

Active damping is considered first. Suppose that the rotor transverse displacement is measured at the node indicated by the triangle in Figure 1c (and marked by 1 in location vector $\mathbf{l}_d$). Negative position derivative feedback control is implemented by computing a numerical time derivative of measurement $\mathbf{l}_d^T\mathbf{x}^s$, multiplying it by gain k_d, transforming it to the rotating frame and regulating the actuator voltages accordingly (eq. 5):

$$v = -e^{-i\Omega t} k_d \tfrac{d}{dt}(\mathbf{l}_d^T\mathbf{x}^s) \quad \Rightarrow \quad \mathbf{f}_q^s = e^{i\Omega t} K_q \mathbf{l}_q v = -K_q \mathbf{l}_q k_d \tfrac{d}{dt}(\mathbf{l}_d^T\mathbf{x}^s) \approx -\mathbf{C}^q\dot{\mathbf{x}}^s \tag{5}$$

Since rotor-fixed force actuators and stator-fixed displacement sensors are not collocated and numerical differentiation amplifies measurement noise, low-pass filters must be used in practice to avoid high frequency destabilization and noise amplification.

To obtain the rotor response to unbalance, a nodal unbalance vector **e** is computed on the basis of assumed nodal eccentricities: 2μm at the four nodes of the flywheel and 2μm perpendicular to it at the node at the mid piece other end. The actuation voltages required to cancel the resulting modal unbalance are 325V and 429V at the first and second critical speeds, respectively, which is attainable. The response to unbalance **z** is computed in terms of forward and backward rotating vectors $\mathbf{x}^m$ and $\mathbf{x}^d$ by inverting the dynamic matrix $\mathbf{D}(\Omega)$ of a rotor system with anisotropic stator stiffness and viscous damping as described by eq.6:

$$\mathbf{z} = \mathbf{D}(\Omega)^{-1}\mathbf{f} \qquad \mathbf{z} = \begin{Bmatrix}\mathbf{x}^m \\ \overline{\mathbf{x}}^d\end{Bmatrix} \qquad \mathbf{f} = \begin{Bmatrix}\Omega^2\mathbf{e} \\ \mathbf{0}\end{Bmatrix} \qquad \mathbf{C}^q = -K_q\mathbf{l}_q k_d \mathbf{l}_d^T$$
$$\mathbf{D}(\Omega) = \begin{bmatrix} -\Omega^2(\mathbf{M}^m - \mathbf{G}) + i\Omega(\mathbf{C}^m + \mathbf{C}^q) + \mathbf{K}^m & i\Omega\mathbf{C}^{sd} + \mathbf{K}^{sd} \\ i\Omega\mathbf{C}^{sd} + \mathbf{K}^{sd} & -\Omega^2(\mathbf{M}^m + \mathbf{G}) + i\Omega(\mathbf{C}^m + \mathbf{C}^q + 2\mathbf{C}^r) + \mathbf{K}^m \end{bmatrix} \tag{6}$$

The displacement response to unbalance in the absence of control is shown in Figure 4. The maximum displacement occurs as forward motion at the fourth critical speed. If derivative feedback control is applied, this maximum response is reduced by some 90% for the chosen feedback gain. Note that active damping effectively merges the closely spaced resonance frequencies which are due to stator stiffness anisotropy, such that the response becomes similar to that of a well-damped axi-symmetric rotor system.

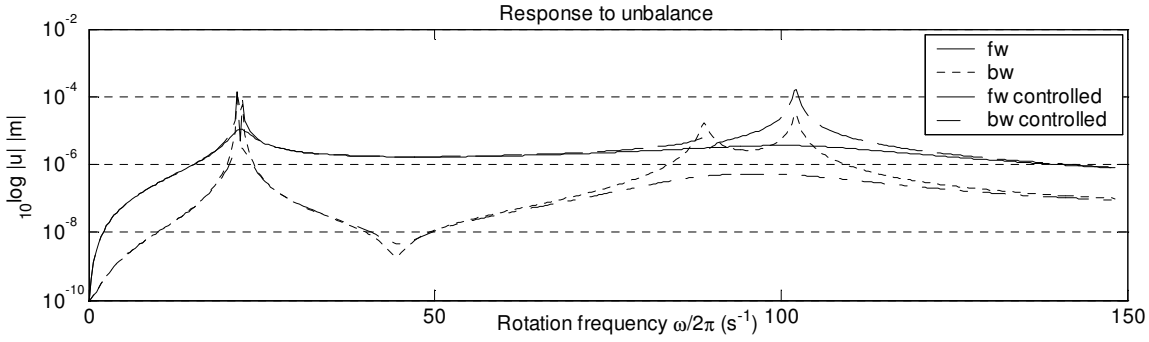

Figure 4. Unbalance response with and without control.

3.3 Preparatory experiments with speed-scheduled unbalance compensation

The setup considered in the preceding sections is not yet ready for high speed experiments. Speed-scheduled algorithms for the suppression of unbalance induced vibration are therefore evaluated for a setup with a light weight drive shaft, which has length 1m and 10x10 mm square cross-section (Figure 5a). The stator of this setup is axi-symmetric, while the shaft is symmetric with respect to three orthogonal planes. Thin monolithic piezoceramic plates are mounted to the shaft surface; their voltage is controlled by voltage amplifiers via a slipring assembly. The speed is regulated so as to increase linearly from 0 to 50 revolutions per second in 30s. At the first critical speed of 25.4 revolutions per second, the first bending mode vibration is limited by a catcher bearing at midshaft to 3.9mm (see Figure 5b).

A speed-dependent algorithm for active balancing is evaluated. It consists of three parts: 1) estimation of modal unbalance using the inverse modal stiffness at speeds significantly below the critical speed (while δ_e is high in Figure 5c), 2) active balancing by the application of a constant voltage at speeds near and above the critical speed (while δ_b is high in Figure 5c) and 3) low-pass filtered velocity feedback near the critical speed (while δ_d is high in Figure 5c). The actuation voltages are shown at the top of Figure 5c. The maximum displacement at midshaft is reduced from 3800µm to less than 120µm at the critical speed - a reduction of 97% - while the response to unbalance is reduced at supercritical speeds as well.

The considered approach gives rise to slowly changing actuation voltages, because the compensation of modal unbalance is in fact achieved by rotor shape control. Slowly changing voltages can also be used if the stator stiffness is anisotropic, because slightly different bending modes are excited by largely the same part of the unbalance distribution. Only very little energy (~0.34mJ) is required to balance a single bending mode. Balancing devices which are powered by ambient light or rotor straining under gravity should hence be feasible.

The relevance of electric dissipation of strain induced currents (see 3.1) is determined for this setup as well. To this end, the stator damping is reduced by removing damping layers. The first bending mode vibration may then be changed from stable to unstable by modifying the passive electric boundary conditions of the actuators. A case where the rotor is only marginally stable at supercritical speeds is shown in Figure 5d. The conclusion from this experiment is equal to that from section 3.1: the electric circuits connected to rotor-fixed actuators should be designed so as to avoid significant dissipation. It is remarked that heavy rotors with comparably little piezoelectric actuator material are less prone to destabilization.

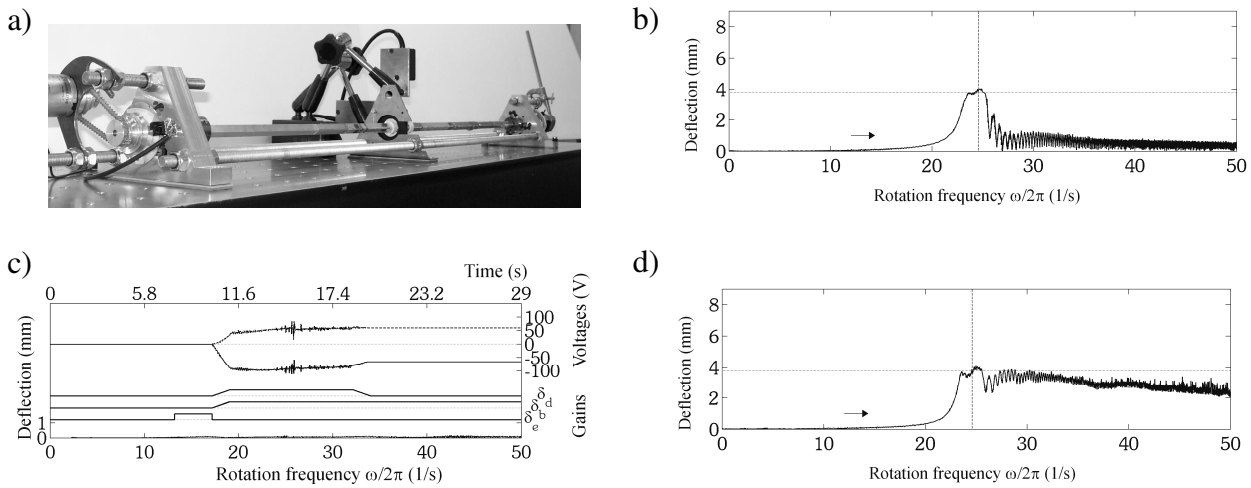

Figure 5. a) Light-weight drive shaft setup. b) Unbalance response of uncontrolled rotor system. c) Voltages, scheduling gains δ_d, δ_b and δ_e and unbalance response of actively controlled rotor system. d) Instability due to low stator damping and resistive dissipation of strain induced currents.

4. MASS ACTUATION

4.1 Unbalance compensation

Rotor systems which pass several critical speeds during a run can be balanced with a single balancing device if a speed-dependent algorithm is used to switch between active balancing of different modes ([9]). The balancing device should have a low positioning time, because an accurate estimate of modal unbalance can be obtained only while the rotor speed approaches a critical speed, whereas active balancing must be performed while the speed is still sufficiently far from this critical speed to avoid a large transient response due to the balancer movement.

In contrast with force actuators that often have a rather limited force capability, mass redistribution actuators can compensate large amounts of unbalance. Suppose that the unbalance distribution is ten times that assumed in section 3. The resulting modal unbalance can be compensated at the position of the PUM mass actuator by $65 \cdot 10^{-6}$ kgm at the first critical speed and $10 \cdot 10^{-6}$ kgm at the second. A controllable unbalance of $65 \cdot 10^{-6}$ kgm can be realized by fixing weights of $2.2 \cdot 10^{-3}$ kg at the outer radius of both balancer rings.

4.2 Experimental actuator characterization

The proposed mass redistribution device is manufactured by enlarging the inner diameter of two ultrasonic motors to ∅15mm and mounting two balancer rings at sliding bearings with slightly flexible supports (Figure 6). In experiments, this device is used with and without a balancer weight of $3.0 \cdot 10^{-3}$ kg attached. The motor speed is set to the maximum value attainable and the rotation angle of one ring is measured using a laser distance sensor. Three reference functions are specified which switch between 0 and 52, 26 and 13 degrees, respectively. The references are realized by switching the power for forward and backward motion on and off. The resulting angles and angular speeds are shown in Figure 7.

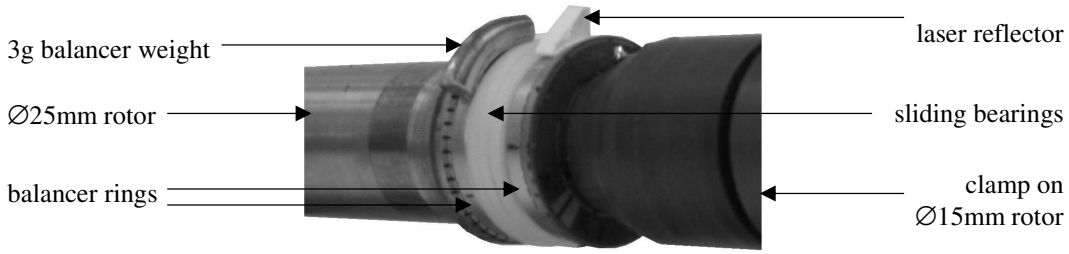

Figure 6. Experimental PUM mass actuator device mounted to a flexible rotor.

With no balancer weight attached, a maximum speed of 1400 deg/s is reached within 3ms. With the 3g balancer weight attached and accelerated opposite to gravity, a maximum speed of 800 deg/s is reached within 5ms. It follows that the mass actuator can realize any angular position in less than 230ms. Taking into consideration that accurate angle control at low speeds is possible by regulating the relative phase of the actuation voltages (see [5]), it is concluded that use of the PUM device as mass redistribution actuator is promising.

In certain cases, the device might also be used as dynamic exciter for identification purposes. With no balancer weight attached, a reference switching between 0 and 13 degrees can be realized 33 times per second (see last plot of Figure 7). However, such high frequencies cannot be realized without considerable slip if the 3g balancer weight is attached. Hence, the use of this actuator as dynamic exciter is possible only at very low frequencies.

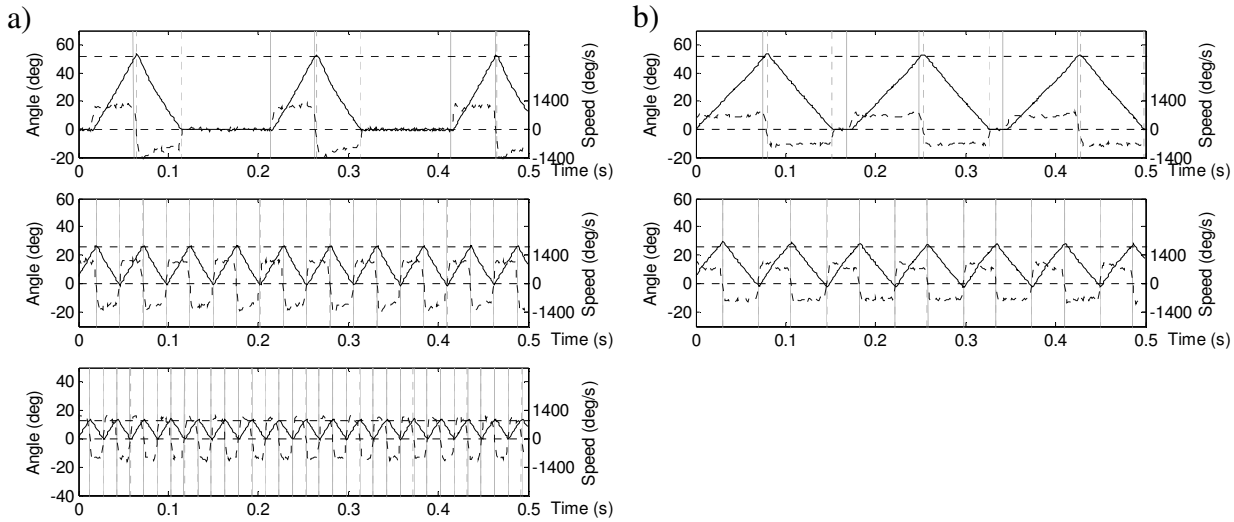

Figure 7. PUM response, balancer weight: a) absent, b) present. Black lines: angle (—), angular speed (····), reference (- -). Gray lines: switching of power for forward (—) and backward (····) motion.

5. CONCLUSIONS

Two innovative actuators for rotor vibration control are investigated using simulations and experiments. Piezoceramic force actuators are found to be very attractive for active vibration control of flexible rotors and for active balancing in particular. Piezoelectric ultrasonic motors are found to be promising for active balancing of high speed rotors. Future research will focus on the co-simulation of electronics for piezoelectric force actuators, on accurate angle control of piezoelectric ultrasonic motors, on miniature non-contact power supplies for both devices and on improved control algorithms that make use of iterative learning.

REFERENCES

[1] S. Zhou, J. Shi, "Active balancing and vibration control of rotating machinery: a survey", *The Shock and Vibration Digest* **33**(4), 361-371 (2001).

[2] G. Genta, *Dynamics of Rotating Systems,* Politecnico di Torino, Springer Science+Business Media, Inc., 2005.

[3] C.-W. Lee, *Vibration Analysis of Rotors*, Kluwer Academic Publishers, Dordrecht, 1993.

[4] J. L. Pons, H. Rodríguez, F. Seco, R. Ceres, L. Calderón, "Modelling of piezoelectric transducers applied to piezoelectric motors: a comparative study and new perspective", *Sensors and Actuators A* **110**, 336-343 (2004).

[5] F. Giraud, B. Lemaire-Semail, J. Aragones, J. Robineau, "Precise position control of a travelling wave ultrasonic motor", IEEE IAS2005, October 2, 2005.

[6] C. J. Cross, S. Fleeter, "Shunted piezoelectric for passive control of turbomachine blading flow-induced vibrations", Smart Materials and Structures **11**, 239-248 (2002).

[7] H.-G. Horst, H. P. Wölfel, "Active vibration control of a high-speed rotor using PZT patches on the shaft surface", *Journal of Intelligent Material Systems and Structures* **15**(9):721-728.

[8] H. Kunze, M. Riedel, K. Schmidt, E. Bianchini, "Vibration reduction on automotive shafts using piezoceramics", *Proceedings of SPIE*, 5054:382-386.

[9] S. Zhou, J. Shi, "Optimal one-plane active balancing of a rigid rotor during acceleration", *Journal of Sound and Vibration* **249**(1):196-205.